(21) E. Stenhagen, S. Abrahamsson, and F. W. McLafferty, "Registry of Mass Spectral Data", Wiley, New York, 1974.
(22) E. Herbst, J. M. Norbeck, P. R. Certain, and W. Klemperer, *Astrophys. J.*, **207**, 109 (1976).
(23) P. J. Bruna, S. D. Peyerimhoff, and R. J. Buenker, *Chem. Phys.*, **10**, 323 (1975).
(24) A. Cornu and R. Massot, "Compilation of Mass Spectral Data", Heyden & Sons, London, 1966.
(25) R. C. Bingham, M. J. S. Dewar, and D. H. Lo, *J. Am. Chem. Soc.*, **97**, 1285 (1975).
(26) W. J. Hehre, R. F. Stewart, and J. A. Pople, *J. Chem. Phys.*, **51**, 2657 (1969).
(27) W. J. Hehre, R. Ditchfield, R. F. Stewart, and J. A. Pople, *J. Chem. Phys.*, **52**, 2191 (1970).
(28) "Tables of Interatomic Distances and Configuration in Molecules and Ions," *Chem. Soc., Spec. Publ.*, **No. 11**, M107, M109 (1958); *Suppl.*, **No. 18**, M62S (1965).
(29) R. Ditchfield, W. J. Hehre, and J. A. Pople, *J. Chem. Phys.*, **54**, 724 (1971).
(30) W. J. Hehre and W. A. Lathan, *J. Chem. Phys.*, **56**, 5255 (1972).
(31) T. Keough, J. H. Beynon, and R. G. Cooks, *Int. J. Mass Spectrom. Ion Phys.*, **16**, 417 (1975).

Gas-Phase Ion–Molecule Association Reactions. A Statistical Phase Space Theory Approach

Lewis Bass, Walter J. Chesnavich, and Michael T. Bowers*

Contribution from the Department of Chemistry, University of California, Santa Barbara, California 93106. *Received February 8, 1979*

Abstract: A theoretical treatment of gas-phase ion-molecule association reactions is presented. The treatment is developed for the energy-transfer model $AH^+ + A \rightleftarrows (A_2H^+)^*$; $(A_2H^+)^* + A \rightarrow A_2H^+ + A$. Explicit distribution functions for the activating reaction and for the steady-state distribution of $(A_2H^+)^*$ are presented. The phase space theory technique utilized rigorously conserves energy and angular momentum. Unimolecular reaction of $(A_2H^+)^*$ is shown to depend strongly on angular momentum. Detailed comparison between theory and experiment is made for A = NH_3, CH_3NH_2, $(CH_3)_2NH$, and $(CH_3)_3N$ over a wide range of temperature and pressure. The phase space theory results give semiquantitative agreement with experiment for all systems except possibly NH_3. The mechanism of the reaction is discussed in detail.

I. Introduction

Statistical approaches to reaction rate theory are well established as useful tools in understanding rates and mechanisms of chemical reactions. Useful summaries of the development of the theory as applied to unimolecular reactions have been presented by Robinson and Holbrook[1a] and by Forst.[1b] The central focus of the theory is the calculation of the microscopic rate constant for unimolecular fragmentation from a given reactant state. To obtain macroscopic rates for comparison with experiments the microscopic rates are incorporated into the details of the particular reaction mechanism being studied. For example, the application of statistical theory to the association reaction

$$AH^+ + A \xrightarrow{k_2} A_2H^+ \tag{1}$$

may be accomplished by use of the chemical activation mechanism

$$AH^+ + A \underset{\bar{k}_b}{\overset{k_f}{\rightleftharpoons}} (A_2H^+)^* \xrightarrow{k_s[A]} A_2H^+ \tag{2}$$

This mechanism has recently been invoked by Meot-Ner and Field[2] and Neilson et al.[3] to characterize the dimerization kinetics of ammonium ions in ammonia and the methylamines. With the assumption that $(A_2H^+)^*$ is in a steady state the kinetics yield

$$k_2 = \frac{k_f\omega}{\bar{k}_b + \omega} \tag{3a}$$

or

$$\frac{1}{k_2} = \frac{1}{k_f} + \frac{\bar{k}_b}{k_f\omega} \tag{3b}$$

where the substitution $k_s[A] = \omega$ has been made. Equation 3 may be used to obtain values of $\bar{k}_b$ from measured values of k_2 and estimated values of k_f and k_s. For the amine systems in reaction 2 the following assumptions are commonly used to estimate k_f and k_s: (1) All AH^+/A collisions result in the formation of $(A_2H^+)^*$ complexes. (2) All $(A_2H^+)^*/A$ collisions result in stabilized A_2H^+, i.e., the "strong collision" assumption. (3) The ion–molecule collision rates in (1) and (2) are governed by the long-range term in the potential and are therefore given by Langevin[4] or ADO[5] theory. These three assumptions also lay the groundwork for the calculation of theoretical k_2 values from[1]

$$k_2 = \iint \left[\frac{k_f\omega}{k_b(E,\mathcal{J}) + \omega}\right] F(E,\mathcal{J})\, dE\, d\mathcal{J} \tag{4}$$

where $F(E,\mathcal{J})$ is the distribution function for the activating reaction that forms $(A_2H^+)^*$ and $k_b(E,\mathcal{J})$ is the microscopic rate constant for dissociation of $(A_2H^+)^*$ at energy E and angular momentum $\mathcal{J}$. According to statistical theory the basis for the calculation of $k_b(E,\mathcal{J})$ is embodied in the following two assumptions: (1) The rate of reaction is governed by passage through a transition state located along the reaction coordinate at the point of minimum flux on the system potential energy hypersurface. (2) The decomposing molecule reaches a state of quasi-equilibrium before decomposing; i.e., all energy accessible states in the system phase space have equal probabilities of being populated. Within this framework the microscopic decomposition rate constant for a molecule with available internal energy E above the threshold for reaction and with angular momentum $\mathcal{J}$ is

$$k(E,\mathcal{J}) = \frac{\text{flux}(E,\mathcal{J})}{\rho(E,\mathcal{J})} \tag{5}$$

That is, the rate constant is the ratio of the flux at the transition state to the density of states of the reacting molecule.

In the most extensively used formulation of statistical theory, called RRKM[6] when applied to neutral systems and QET[7] when applied to ionic systems, eq 5 is written more explicitly as

0002-7863/79/1501-5493$01.00/0

$$k(E,\mathcal{J}) = \frac{\sigma W^{\ddagger}(E^*)}{\sigma^{\ddagger} h\rho(E^* + E_0 + E_J^* - E_J)} \quad (6)$$

where E_0 is the reaction threshold energy at $\mathcal{J} = 0$, E_J^* and E_J are the adiabatic rotational energies of the transition state and the reactant molecule, respectively, and $W^{\ddagger}(E^*)$ is the sum of states at the transition state. The symmetry numbers σ and $\sigma^{\ddagger}$, for the reactant molecule and the transition state, respectively, have been shown explicitly for clarity. The sum and density of states are calculated from specified structures and vibrational mode frequencies of the reactant molecule and the transition state; the procedures are well known.[1] Olmstead et al.[8] have applied RRKM theory to the chemical activation system (2) using the assumption that the transition state for the dissociation reaction is located at the maximum in the centrifugal barrier (when the transition state is located at this point, RRKM and QET also become equivalent to "phase space" theory). Good agreement was obtained with the data of Meot-Ner and Field[2] on the amine systems.

One of the disadvantages of RRKM theory is the failure to rigorously conserve angular momentum. A loose transition state located at the centrifugal barrier will consist of two essentially separated fragments, each having rotational energy and rotational angular momentum. These independent rotations, which combine with the orbital angular momentum resulting from the relative motion of the two fragments about each other to form the total angular momentum of the system, are only treated approximately in eq 6. A theory developed by Light and co-workers[9a] and Nikitin[9b] for atom–diatom systems and extended by Chesnavich and Bowers[10] to polyatomic systems addresses this point. In essence, the only difference between phase space theory and "loose" RRKM theory is that the former accounts rigorously for all angular momentum states of the system, including the rotation of the separated fragments. Under this restriction, and under the assumption that A_2H^+ is a spherical top, the microscopic dissociation rate constant becomes

$$k_b(E,\mathcal{J}) = \frac{\sigma_{A_2H^+}}{\sigma_A \sigma_{AH^+} h} \frac{\int_{\mathcal{E}^{\ddagger}_{tr}}^{E} \Gamma(\mathcal{E}_{tr},\mathcal{J})\rho_v(E - \mathcal{E}_{tr})\, d\mathcal{E}_{tr}}{(2\mathcal{J})\rho_v'(E + E_0 - B\mathcal{J}^2)} \quad (7)$$

where $\Gamma(\mathcal{E}_{tr},\mathcal{J})$ is the sum of rotational-orbital states of the separated fragments at translational-rotational energy $\mathcal{E}_{tr}$, $\mathcal{E}^{\ddagger}_{tr}$ is the smallest value of $\mathcal{E}_{tr}$ for which the separating fragments can overcome the centrifugal barrier and indeed separate, $\rho_v(E - \mathcal{E}_{tr})$ is the vibrational density of states of the fragments at vibrational energy $E - \mathcal{E}_{tr}$, $\rho_v'(E + E_0 - B\mathcal{J}^2)$ is the vibrational density of states of the A_2H^+ complex at vibrational energy $E + E_0 - B\mathcal{J}^2$, B is the rotational constant of the complex, and $2\mathcal{J}$ is the rotational spatial degeneracy of the complex at angular momentum $\mathcal{J}$. This equation, with rigorous conservation of angular momentum, should prove more accurate than eq 6 for systems dominated by the centrifugal potential. The discrepancy between the two treatments will be greater for states with larger angular momentum. The final comparison of macroscopic rates predicted by the two theories will depend on the distribution function which describes the relative importance of states with high and low angular momentum.

In this paper the "phase space" theory rate constant in eq 7 is used to describe the dissociation step in the chemical activation system (2). By combining $k_b(E,\mathcal{J})$ with the estimated values of k_f and k_s the steady-state distribution function for energy and angular momentum in the A_2H^+ complex is obtained. This distribution function, which depends on temperature and pressure, is then employed in the calculation of k_2 and $\bar{k}_b$ values for comparison with experimental results. Thus, the effects of temperature and pressure on the rate constant may be examined by studying the interrelationship of the distribution function and the microscopic rate constant in determining the average rate. The amine systems which will be discussed here have been chosen because the dynamics of complex formation and dissociation is expected to be governed by the centrifugal potential, complex formation is expected to occur with large values of angular momentum (due to the relatively large impact parameters which ion-molecule collisions may have), and comparison can be made with the experiments of Meot-Ner and Field[2] and the RRKM calculations of Olmstead et al.[8] in the 1 Torr pressure regime, and with the recently published ICR data of Neilson et al.[3] obtained at 10^{-4}–10^{-3} Torr.

The paper is organized as follows. In section II the theory is briefly discussed, presenting the equations necessary for the calculation of the distribution function and rate constants. In section III the results of the calculations are presented in terms of general trends resulting from the theory, and in terms of specific comparisons with experimental results for the four amine systems. Section IV discusses in detail the comparisons between theory and experiment and the resulting conclusions concerning the reaction mechanism. The details of the parameters used to characterize the amine systems are presented in the Appendix.

II. Theory

A schematic of the reaction surface that serves to define the energies is shown in Figure 1. In addition to these energy parameters, the various contributions to the angular momentum must be specified. The A_2H^+ complex has only rotational angular momentum $\vec{\mathcal{J}}$, while the separated fragments contain orbital angular momentum $\mathbf{L}$ in addition to their independent rotational angular momenta $\mathbf{J}_A$ and $\mathbf{J}_{AH^+}$. Conservation of angular momentum and energy is expressed by the equations

$$\vec{\mathcal{J}} = \mathbf{J}_A + \mathbf{J}_{AH^+} + \mathbf{L} = \mathbf{J}_r + \mathbf{L} \quad (8a)$$

$$E + E_0 = \mathcal{E}_t + \mathcal{E}_r + \mathcal{E}_v = \mathcal{E}_{tr} + \mathcal{E}_v \quad (8b)$$

$$E + E_0 = \mathcal{E}_r' + \mathcal{E}_v' \quad (8c)$$

where the primed quantities refer to the A_2H^+ species and the subscripts r, v, and t represent rotational, vibrational, and relative translational motion, respectively. Note that $\mathcal{E}_r$ and $\mathcal{E}_v$ contain contributions from both A and AH^+. The application of eq 8 to evaluate sums and densities of states for collision pairs has been discussed in detail by Chesnavich and Bowers.[10] In this work all rotational motion is treated as the classical rotation of a spherical top. Chesnavich and Bowers[10] have demonstrated that the error introduced by this approximation is slight.

Before eq 4 can be used to calculate k_2 an expression for $F(E,\mathcal{J})$ must be obtained. This distribution function describes the activating reaction and can thus be calculated from the relative rates of activation into each $(E,\mathcal{J})$ state.[1] Consider the case in which the collision partners A and AH^+ are both in the ground vibrational state. Then the collision rate at energy $\mathcal{E}_{tr}$ and angular momentum $\mathcal{J}$ is proportional to the flux of collision pairs across the centrifugal barrier, given by $\Gamma(\mathcal{E}_{tr},\mathcal{J})/h$.[10] The distribution function is obtained by multiplying the flux by the thermal $2\mathcal{J}e^{-\mathcal{E}_{tr}/kT}$ weighting factor and normalizing:

$$F_{tr}(\mathcal{E}_{tr},\mathcal{J}) = \frac{\Gamma(\mathcal{E}_{tr},\mathcal{J})2\mathcal{J}e^{-\mathcal{E}_{tr}/kT}}{\int_{\mathcal{E}_{tr}=0}^{\infty}\int_{\mathcal{J}=0}^{\mathcal{J}_{max}} \Gamma(\mathcal{E}_{tr},\mathcal{J})2\mathcal{J}e^{-\mathcal{E}_{tr}/kT}\, d\mathcal{J}\, d\mathcal{E}_{tr}} \quad (9)$$

where the subscript tr indicates that only the translational-rotational energy has been considered. To include vibrational

energy the appropriate density of states must be included and the flux integrated over all possible values of the translational-rotational energy:

$$F(E,\mathscr{J}) = \frac{2\mathscr{J}e^{-E/kT}\int_{\mathscr{E}^{\ddagger}_{tr}}^{E}\Gamma(\mathscr{E}_{tr},\mathscr{J})\rho_v(E-\mathscr{E}_{tr})\,d\mathscr{E}_{tr}}{\int_{E=0}^{\infty}\int_{\mathscr{J}=0}^{\mathscr{J}_{max}}2\mathscr{J}e^{-\mathscr{E}_{tr}/kT}\int_{\mathscr{E}^{\ddagger}_{tr}}^{E}\Gamma(\mathscr{E}_{tr},\mathscr{J}) \times \rho_v(E-\mathscr{E}_{tr})\,d\mathscr{E}_{tr}\,d\mathscr{J}\,dE} \quad (10)$$

$\mathscr{J}_{max}$ is determined by the smaller of two independent limiting values. The first limit depends on the total energy of the complex and is simply a statement of the fact that the rotational energy cannot exceed the total energy. Thus

$$\mathscr{J} \le \left(\frac{E+E_0}{B}\right)^{1/2} \equiv \mathscr{J}_E^* \quad (11)$$

where B is the rotational constant of the A_2H^+ complex. The second limit is determined by the details of the collision process, rather than the properties of the complex. The relative kinetic energy of the collision pair determines a maximum orbital angular momentum for which an ion–molecular pair can overcome the centrifugal barrier and form a collision complex. For the charge-induced dipole potential this maximum is given by eq 12a[10]

$$L^* = (\Lambda\mathscr{E}_t)^{1/4} \quad (12a)$$

$$\Lambda = 8q^2\alpha\mu^2/\hbar^4 \quad (12b)$$

where q is the charge on the ion, α is the polarizability of the neutral, and μ is the reduced mass of the collision pair. The total rotational energy of the separated fragments determines an upper limit on the resulting (classical) total rotational angular momentum, given by the equation

$$J_r^* = (\mathscr{E}_r/B_r)^{1/2} \quad (13)$$

where B_r is the reduced rotational constant

$$B_r = \frac{B_A B_{AH^+}}{B_A + B_{AH^+}} \quad (14)$$

Equations 12 and 13 can be combined to yield the maximum $\mathscr{J}$ at a given $\mathscr{E}_t$ and $\mathscr{E}_r$:

$$\mathscr{J}'(\mathscr{E}_t,\mathscr{E}_r) = J_r^* + L^* = (\mathscr{E}_r/B_r)^{1/2} + (\Lambda\mathscr{E}_t)^{1/4} \quad (15)$$

To determine the maximum $\mathscr{J}$ at a given total energy E eq 15 is maximized with respect to $\mathscr{E}_t$ under the restriction that $\mathscr{E}_t + \mathscr{E}_r = E$, i.e., the vibrational energy is set to zero, as it logically must be in order for the angular momentum to reach a maximum. The resulting derivative, given by

$$\left(\frac{d\mathscr{J}'(\mathscr{E}_t,\mathscr{E}_r)}{d\mathscr{E}_t}\right)_E = \frac{\Lambda}{4}(\Lambda\mathscr{E}_t)^{-3/4} - \frac{1}{2B_r}\left(\frac{E-\mathscr{E}_t}{B_r}\right)^{-1/2} \quad (16)$$

is set to zero and solved numerically for $\mathscr{E}_t$. This value of $\mathscr{E}_t$ is inserted into eq 15 to determine the collision-limited maximum value of $\mathscr{J}$, denoted $\mathscr{J}_C^*$. Since $\mathscr{J}$ must always be less than both $\mathscr{J}_C^*$ and $\mathscr{J}_E^*$, $\mathscr{J}_{max}$ is given formally by

$$\mathscr{J}_{max} = \text{lesser of } (\mathscr{J}_E^*, \mathscr{J}_C^*) \quad (17)$$

In addition to the calculation of k_2 it is desirable to calculate macroscopic dissociation rate constants for comparison with experiment. This is accomplished by averaging $k_b(E,\mathscr{J})$ in eq 7 over the appropriate $(E,\mathscr{J})$ distribution function which characterizes the A_2H^+ ensemble at steady state. A simple mass balance applied to a given $(E,\mathscr{J})$ state in reaction 2 at steady state yields

$$P'(E,\mathscr{J})_{ss} = \frac{k_f F(E,\mathscr{J})[A][AH^+]}{k_b(E,\mathscr{J}) + \omega} \quad (18)$$

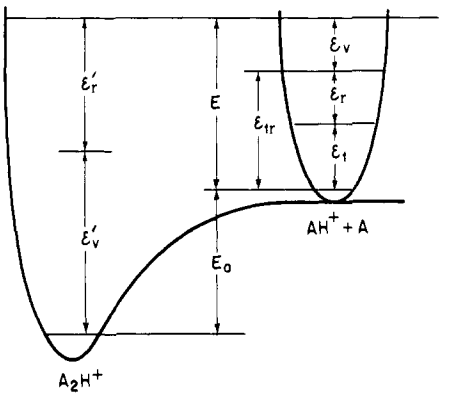

Figure 1. Schematic energy surface showing the energy quantities of interest.

where $P'(E,\mathscr{J})_{ss}$ is, strictly speaking, the steady-state concentration of A_2H^+ in state $(E,\mathscr{J})$. This can be converted to a distribution function by normalizing

$$P(E,\mathscr{J})_{ss} = \frac{\dfrac{F(E,\mathscr{J})}{k_b(E,\mathscr{J})+\omega}}{\displaystyle\int_{E=0}^{\infty}\int_{\mathscr{J}=0}^{\mathscr{J}_{max}}\frac{F(E,\mathscr{J})}{k_b(E,\mathscr{J})+\omega}\,d\mathscr{J}\,dE} \quad (19)$$

The average dissociation rate constant is then given by

$$\bar{k}_b = \int_{E=0}^{\infty}\int_{\mathscr{J}=0}^{\mathscr{J}_{max}} k_b(E,\mathscr{J})P(E,\mathscr{J})_{ss}\,d\mathscr{J}\,dE \quad (20)$$

It should be noted that $P(E,\mathscr{J})_{ss}$ represents a distribution of populations at steady state while $F(E,\mathscr{J})$ represents a distribution of rates of formation.

It is interesting to note that the value of k_2 calculated from eq 4 is exactly equivalent to that calculated by inserting $\bar{k}_b$ from eq 20 into eq 3. This is a statement of the fact that there are two equivalent methods of calculating the fraction of collision complexes which is stabilized as compared to the total number which either are stabilized or decomposed. The first method, that of eq 3, is to average the stabilization and dissociation rates separately over the steady-state distribution function and then calculate the appropriate fraction; the second method, that of eq 4, is to express the fraction stabilized for a given $(E,\mathscr{J})$ state and then average this fraction over the distribution function for the activating reaction. This equivalence is expressed in the equation

$$\frac{\omega}{\langle k_b(E,\mathscr{J})\rangle_{P_{ss}} + \omega} \equiv \left\langle\frac{\omega}{k_b(E,\mathscr{J})+\omega}\right\rangle_F \quad (21)$$

where the brackets indicate averaging over the indicated distribution function.

III. Results

The variation of $k_b(E,\mathscr{J})$ with E and $\mathscr{J}$ is illustrated in Figure 2. The values of the various parameters used in these calculations as well as the remaining calculations are given in the Appendix. The numerical results shown are those calculated for the ammonia dimer from eq 7; the qualitative behavior is characteristic of any unimolecular dissociation described by phase space theory. The most striking aspect of this behavior is the difference in the qualitative nature of the curves at low and at high energy. This change in behavior is a direct result of the change in the relative values of $\mathscr{J}_E^*$ and $\mathscr{J}_C^*$. Recall from the definitions of these two limits that $\Gamma(\mathscr{E}_{tr},\mathscr{J})$ goes to zero at $\mathscr{J}_C^*$ and that $\rho_v'(E_t + E_0 - B\mathscr{J}^2)$ approaches zero but remains finite at $\mathscr{J}_E^*$ (note that if vibrational modes are treated semiclassically then $\rho_v'(E+E_0-B\mathscr{J}^2)$ does fall to zero at $\mathscr{J}_E^*$). At low energy $\mathscr{J}_C^* < \mathscr{J}_E^*$ so $\mathscr{J}_{max}$ is deter-

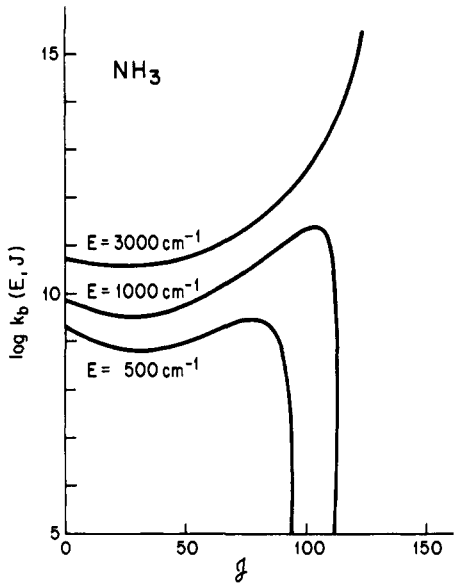

Figure 2. Variation of the microscopic rate constant $k_b(E,\mathcal{J})$ with angular momentum at constant total energy. Calculated for the ammonia dimer at several values of the total energy E.

mined by $\mathcal{J}_C$* and the rate goes to zero at this limit. At high energy $\mathcal{J}_E$* < $\mathcal{J}_C$* and it is $\mathcal{J}_E$* which determines $\mathcal{J}_{max}$. In this case, as $\mathcal{J}$ approaches $\mathcal{J}_{max}$, $\rho_v(E + E_0 - B\mathcal{J}^2)$ falls off much more rapidly than $I(\mathcal{E}_t,\mathcal{J})$. Hence, the rate constant increases rapidly at high $\mathcal{J}$ and reaches a maximum at $\mathcal{J}_{max}$. In the particular case shown in Figure 2 the maximum value of $k_b(E,\mathcal{J})$ at 3000 cm^{-1} is greater than 10^{15} s^{-1} (if vibrational modes are treated semiclassically the rate always becomes infinite at $\mathcal{J} = \mathcal{J}_E$*).

The prediction of such large unimolecular rate constants for high-energy, high-$\mathcal{J}$ states presents a shortcoming of the theory. The quasi-equilibrium assumption becomes tenuous on this time scale as does the entire concept of "collision complex". For example, Neilson et al.[3] have estimated the collision duration for classical scattering of NH_4^+ colliding with NH_3 to be 5×10^{-13} s. High $E,\mathcal{J}$ states become important as temperature is increased and, for the collisional activation mechanism discussed here, as pressure is increased. Thus, the present form of the theory should be applied with caution under these circumstances. Fortunately, as will become apparent shortly, the high $E,\mathcal{J}$ states that lead to physically unrealistic values of $k_b(E,\mathcal{J})$ do not contribute in a significant way to the thermal energy (200-600 K) and low-pressure (0-10 Torr) regimes discussed in this paper. For higher temperatures and pressures and for other reaction mechanisms the theory may have to be modified. One modification would be to include other terms in the potential—in particular a repulsive term could be of importance. This term will have the effect of reducing the contribution of high $E,\mathcal{J}$ states due to modification of the capture criteria. A second modification could be inclusion of centrifugal distortion corrections. This modification would have the effect of siphoning energy from rotation to vibration in the high $\mathcal{J}$ states and thus reduce the value of $k_b(E,\mathcal{J})$ associated with these states.

One other aspect of the curves in Figure 2 should be emphasized. Even for relatively low energies, $k_b(E,\mathcal{J})$ displays a strong dependence on $\mathcal{J}$. For E = 500 cm^{-1} $k_b(E,\mathcal{J})$ varies by about an order of magnitude as $\mathcal{J}$ varies from 0 to $\mathcal{J}_{max}$ and at E = 1000 cm^{-1} $k_b(E,\mathcal{J})$ varies by nearly two orders of magnitude. The fact that $k_b(E,\mathcal{J})$ first decreases with increasing $\mathcal{J}$, goes through a minimum, and then increases results from the detailed variation of the numerator and denominator in eq 7 as $\mathcal{J}$ varies.

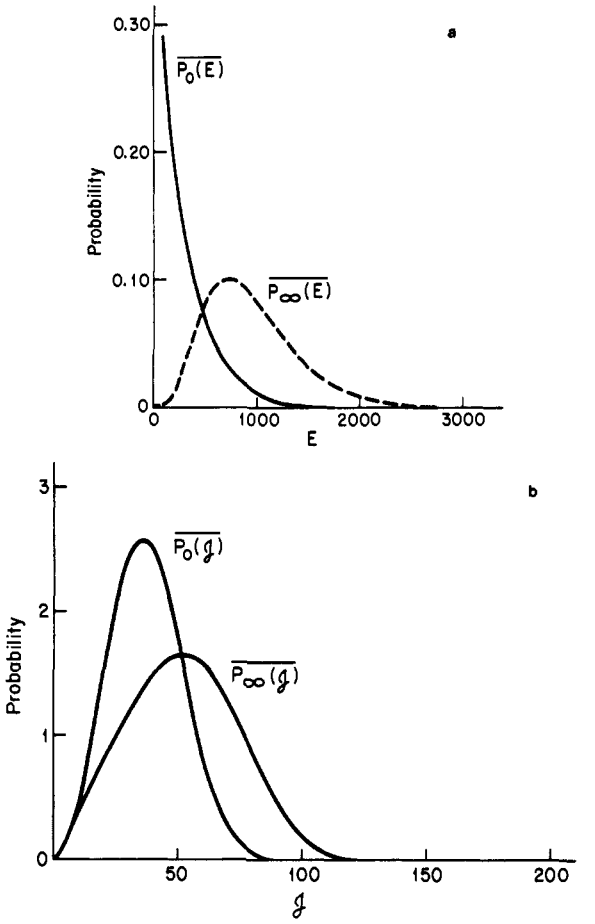

Figure 3. Steady-state distribution function for $(NH_3)_2H^+$ at 300 K, at the zero and infinite pressure limits: (a) energy distribution; (b) angular momentum distribution.

The effects of temperature and pressure on the steady-state distribution function can be seen from examination of eq 9 and 19. Increased temperature shifts the distribution to higher

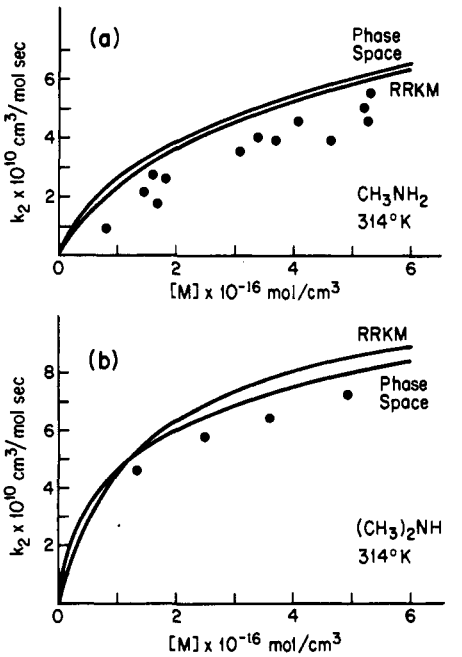

Figure 4. Comparison of theoretical and experimental values of k_2 as a function of pressure in the 1 Torr pressure regime. RRKM theory—ref 8; experimental points (●) from ref 2. (a) CH_3NH_2 at 314 K; (b) $(CH_3)_2NH$ at 314 K.

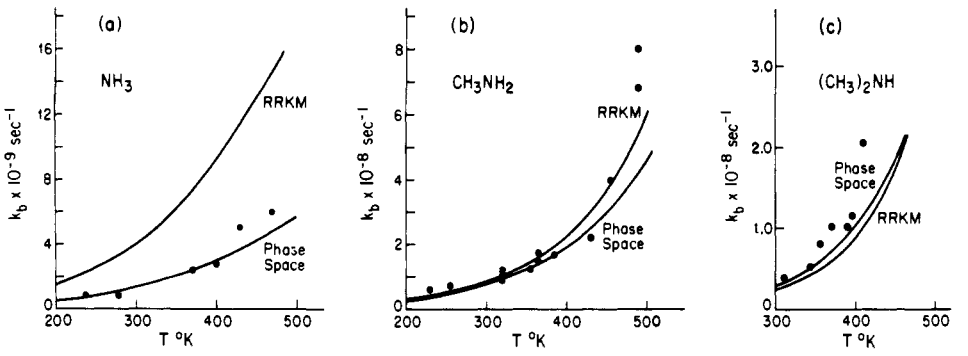

Figure 5. Comparison of theoretical and experimental values of $\bar{k}_b$ as a function of temperature in the 1 Torr pressure regime. Theoretical curves calculated for $\omega = 3.0 \times 10^8\ s^{-1}$. (See Figure 4 for references.)

energies through its effect on $F(E,\mathcal{J})$, i.e., its effect on the thermal energy of the colliding species. Increased pressure shifts the distribution toward $(E,\mathcal{J})$ states with short lifetimes (high $k_b(E,\mathcal{J})$ values) by increasing the stabilization rate of the longer lived states. In the limits of zero and infinite pressure the steady-state distribution function in eq 19 reduces to eq 22 and 23, respectively.

$$P_0(E,\mathcal{J}) = \lim_{\omega \to 0} P(E,\mathcal{J})_{ss} \propto (2\mathcal{J})^2 e^{-E/kT} \rho_v'(E + E_0 - B\mathcal{J}^2) \quad (22)$$

$$P_\infty(E,\mathcal{J}) = \lim_{\omega \to \infty} P(E,\mathcal{J})_{ss} = F(E,\mathcal{J}) \quad (23)$$

Note that eq 22 simply describes a thermal Boltzmann distribution of collision complexes, except that energy levels below E_0 are not populated. Thus the steady-state distribution function varies from a "thermal" distribution at zero pressure to the distribution for the activating reaction at infinite pressure. These two limiting forms are shown in Figure 3 for the ammonia dimer at 300 K, where the distribution functions $\overline{P(E)}$ and $\overline{P(\mathcal{J})}$ are defined as

$$\overline{P(E)} = \int_{\mathcal{J}=0}^{\mathcal{J}_{max}} P(E,\mathcal{J})\, d\mathcal{J} \quad (24)$$

$$\overline{P(\mathcal{J})} = \int_{E=0}^{\infty} P(E,\mathcal{J})\, dE \quad (25)$$

Since the energy axis in Figure 3a represents energy above threshold, $P_0(E)$ contains only the tail of the thermal energy distribution.

Care should be taken when using eq 22 or 23 to ensure that the experimental conditions actually meet the requirement that $\omega \to 0$ or $\omega \to \infty$. These limits must be determined by comparison of the collision frequency and the dissociation rate constant. In the zero pressure limit the condition $\omega \ll k_b(E,\mathcal{J})$ must hold over the entire $(E,\mathcal{J})$ manifold produced with substantial populations by the activating reaction. In the infinite pressure limit the reverse condition must hold. A rough indication of approach to these limits can be obtained by comparison of $\bar{k}_b$ and ω since $\bar{k}_b$ will reflect the range of $k_b(E,\mathcal{J})$ values which contribute most significantly to the rate. Of course, the best indication that one of the pressure limits has indeed been reached is that $\bar{k}_b$ remains unchanged as the pressure is further decreased or increased.

Comparisons of theoretical and experimental rate constants are presented in Figures 4–6. Figure 4 contains experimental k_2 values of Meot-Ner and Field[2] (MF) in the pressure range 0.3–1.8 Torr, along with theoretical predictions of the present phase space theory and of the RRKM treatment of Olmstead et al.[8] Figure 5 shows a comparison for $\bar{k}_b$ values in this pressure regime in the temperature range 200–500 K. Figure 6 shows a comparison between experimental k_2 values of Nielson et al.[3] (NBCDA) and the predictions of phase space theory in the pressure range 10^{-4} to 3×10^{-3} Torr. Also shown are the inverse plots used by NBCDA to obtain values of $\bar{k}_b$. The experimental inverse plot is linear in the pressure range shown, an interesting point that will be discussed in the next section of the paper. In general, good agreement between theory and experiment is obtained for both the MF experiments near 1 Torr and the NBCDA experiments at 10^{-4}–10^{-3} Torr. There are some differences between theory and experiment particularly in the NH_3 system at low pressures, and these will be considered further in the Discussion section.

The phase space results, like those of RRKM theory, are

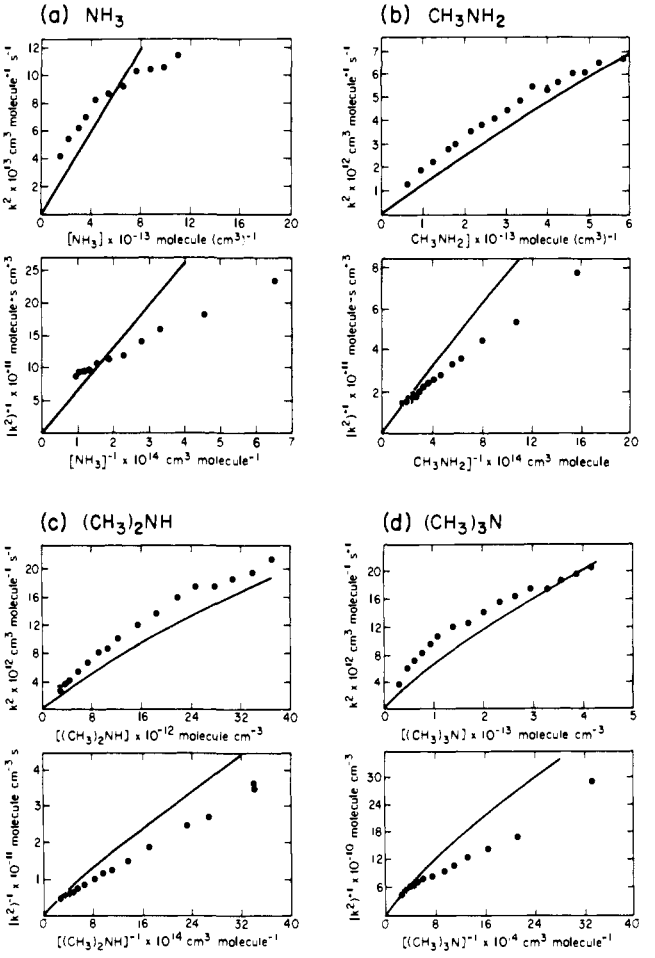

Figure 6. Comparison of theoretical and experimental values of k_2 as a function of pressure in the 10^{-4}–10^{-3} Torr pressure regime (experimental points—ref 3). Also shown are the inverse plots used in ref 3 to obtain $\bar{k}_b$ values.

Table I. Comparison of Experimental and Theoretical Rate Constants (s^{-1})

T, K	expt[a]	theory[b] $\omega \to 0$	theory[b] $\omega = 3.0 \times 10^4$	expt[a]	theory[b] $\omega = 0$	theory[b] $\omega = 3.0 \times 10^4$
195		NH_3			CH_3NH_2	
210	1.2×10^8	3.2×10^8	3.2×10^8	0.5×10^7	0.47×10^7	0.56×10^7
278	4.4×10^8	7.3×10^8	7.4×10^8	1.1×10^7	1.3×10^7	1.5×10^7
302	6.3×10^8	9.4×10^8	9.5×10^8	1.0×10^7	1.8×10^7	2.1×10^7
345				2.1×10^7	3.2×10^7	3.5×10^7
370				3.3×10^7	4.4×10^7	4.8×10^7
		$(CH_3)_2NH$			$(CH_3)_3N$	
195	0.2×10^6	0.21×10^6	0.47×10^6	0.09×10^6	0.05×10^6	0.22×10^6
210				0.10×10^6	0.08×10^6	0.31×10^6
278	0.9×10^6	1.3×10^6	2.2×10^6	0.75×10^6	0.56×10^6	1.5×10^6
302	1.8×10^6	2.1×10^6	3.4×10^6	1.1×10^6	1.1×10^6	2.5×10^6
345	3.4×10^6	4.8×10^6	7.1×10^6	4.5×10^6	3.5×10^6	6.8×10^6
370	7.0×10^6	7.7×10^6	11.0×10^6	5.9×10^6	6.7×10^6	12.0×10^6

[a] From ref 3. [b] See text.

relatively insensitive to the particular choice of parameters used to characterize the (A_2H^+) complex, as long as the resulting calculated values of the entropy change, ΔS, for reaction 1 remains unchanged. For instance, raising the lowest oscillator frequencies from 105 to 200 cm^{-1} (and readjusting the remaining frequencies so that ΔS is unchanged) will affect the calculated value of $\bar{k}_b$ by less than 20%, for temperatures up to 600 K, even at the infinite pressure limit. The choice of the rotational constant, B, of the A_2H^+ complex will have a more pronounced effect on the calculations owing to the role that B plays in determining $\mathscr{J}_E$* according to eq 11 and the resulting effect of $\mathscr{J}_E$* and $\mathscr{J}_C$* on $k_b(E,\mathscr{J})$ values at the upper end of the $(E,\mathscr{J})$ manifold. As was discussed before, the application of the theory to cases where the upper end of the $(E,\mathscr{J})$ manifold is significantly populated will require some modification in order to obtain reasonable $k_b(E,\mathscr{J})$ values for these states. Any such modification which does remedy this situation should also remove the pronounced sensitivity of the calculations to changes in B.

IV. Discussion

There are two kinds of comparisons that can be conveniently made between experiment and theory: apparent values of k_2 vs. pressure and $\bar{k}_b$ vs. temperature or pressure. These points are discussed in sections A and B, respectively. Then there is the general question of the reaction mechanism and the various assumptions in the theory, points discussed in section C. Finally, a very brief comparison is made between the phase space theory results presented here and RRKM theory in section D.

A. k_2 vs. p. The comparison between theory and the experiments of Meot-Ner and Field,[2] Figure 4, is quite good for both the CH_3NH_2 and $(CH_3)_2NH$ systems near 1 Torr pressure. In both cases the theory exceeds experiment but never by more than a factor of 2. The shape of the dependence of k_2 on pressure is reasonably well fit as well.

The comparison between the ICR data of Neilson et al.[3] at 10^{-4}-10^{-3} Torr and theory, Figure 6, is also quite good. The magnitude of k_2 is usually fit to well within a factor of 2 and the shape reasonably well fit for the CH_3NH_2, $(CH_3)_2NH$, and $(CH_3)_3N$ systems. The shape of the curve for the ammonia system is poorly fit, however, and suggests that the assumed energy-transfer mechanism may not adequately describe this system.

B. $\bar{k}_b$ vs. T. Two methods have been used in the literature to obtain experimental values of $\bar{k}_b$. Meot-Ner and Field[2] measured k_2 as a function of T at a fixed pressure. They solved eq 3a for $\bar{k}_b$ and then substituted the experimental values of k_2 and collision-theory values of k_f and k_s to obtain $\bar{k}_b$. The results are plotted in Figure 5 for NH_3, CH_3NH_2, and $(CH_3)_2NH$. Reasonably good agreement between experiment and theory is obtained for all systems.

The second method was employed by Neilson et al.[3] They noted that the plots of k_2^{-1} vs. A^{-1} were linear in the pressure range of their experiments (10^{-4}-10^{-3} Torr) and hence used the slope of these plots (see Figure 6) to obtain $\bar{k}_b$; $\bar{k}_b$ = slope $\times$ $k_f k_s$. These data are summarized in Table I. The question arises how to compare these data to theory. One model is to assume that $\bar{k}_b$ is in the low-pressure limit due to the linearity of the inverse plots, that is, calculate $\bar{k}_b$ at $\omega = 0$. However, since the theoretical value of $\bar{k}_b$ varies with pressure, it is also useful to calculate k_b near the maximum pressure used in the experiments ($\sim 1 \times 10^{-3}$ Torr or $\omega = 3 \times 10^4$ s^{-1}). Both theoretical numbers are included in the table for comparison. If the theory is rigorous and the model correct then the experimental values of $\bar{k}_b$ should be larger than the $\omega = 0$ limit and less than or equal to the $\omega = 3 \times 10^4$ values. This is most nearly the case for $(CH_3)_2NH$ and $(CH_3)_3N$. The experimental values of $\bar{k}_b$ for the CH_3NH_2 system are somewhat lower than the $\omega = 0$ limit and for the NH_3 system they are considerably lower than the $\omega = 0$ limit. A number of reasons might exist for this behavior, including the fact that the CH_3NH_2 system and especially the NH_3 system may not be adequately described by the energy-transfer model.

It is useful to discuss in detail the question of whether inverse plots and their linearity are useful tools for determining rate constants and reaction mechanisms in the gas phase. Consider the plots in Figure 7 for the $(CH_3)_3N$ system. These plots were obtained from phase space theory calculations of $\bar{k}_b$ and are thus purely theoretical. At the lowest pressures (0-2×10^{-6} Torr), Figure 7a, the inverse plot is nearly exactly linear over the entire pressure range. The value of $\bar{k}_b$ obtained from this plot, denoted by the $\to$ on the ordinate, agrees very well with the directly calculated values of $\bar{k}_b$ which are essentially constant over the range. At the highest pressures (0-2×10^{-3} Torr), Figure 7d, the inverse plot is linear over only a portion of the pressure range. The values of $\bar{k}_b$ vary considerably over this range as well. This pressure range most closely resembles the experimental pressures used by Neilson et al. In this case, the linear portion of the inverse plot yields a value of $\bar{k}_b$ somewhere between the zero pressure minimum value and the value at highest pressure. This behavior is mimicked by experiment for the $(CH_3)_2NH$ and $(CH_3)_3N$ systems (Table I). The point is that caution must be employed in using these plots to obtain rate constants and infer reaction mechanisms.

The question arises as to how best to extract experimental values of $\bar{k}_b$ from the data for comparison with theory. One way is analogous to the method used by Meot-Ner and Field discussed earlier. Experimental values of k_2 and theoretical values of k_f and k_s are substituted into eq 3a at each pressure

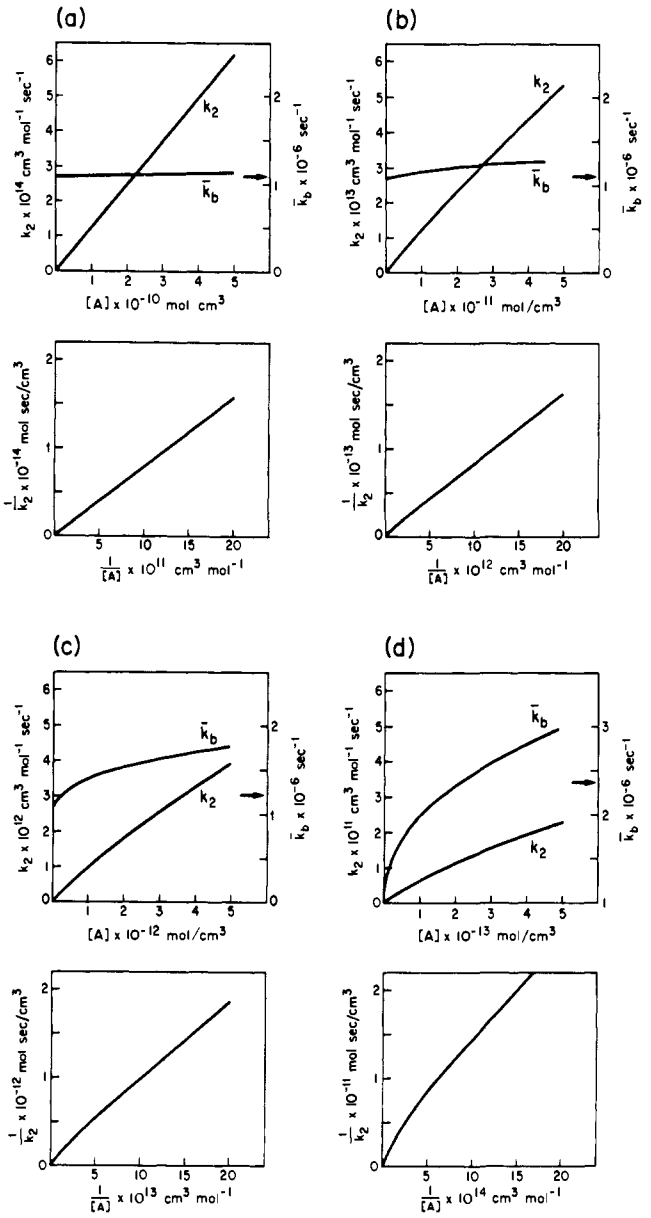

Figure 7. Phase space theory predictions of $\bar{k}_b$ and k_2 as a function of pressure for the $(CH_3)_3N$ system in various pressure regimes. The arrow on the ordinate indicates the value of $\bar{k}_b$ obtained from theoretically predicted inverse plots, which are also shown. See text for discussion.

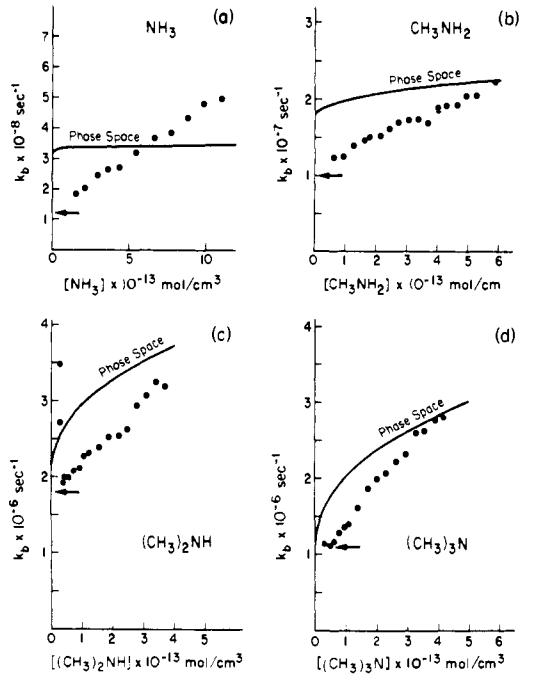

Figure 8. Comparison of theoretical and experimental values of $\bar{k}_b$ as a function of pressure in the 10^{-4}-10^{-3} Torr pressure regime (experimental points—ref 3). Arrows indicate the $\bar{k}_b$ values obtained from the inverse plots in Figure 6.

yielding a value for $\bar{k}_b$ at that pressure. These plots of $\bar{k}_b$ vs. A are compared with theoretical values of $\bar{k}_b$ in Figure 8. Agreement is best for the $(CH_3)_3N$ system, reasonably good for $(CH_3)_2NH$ and CH_3NH_2, and poor for NH_3. One interesting point is that the inverse plot values of $\bar{k}_b$, indicated by the arrows, always provide a lower limit to the experimental values determined directly from eq 3a. It is also interesting to note that the experimental values of $\bar{k}_b$ determined directly from eq 3a increase significantly with pressure as the theoretical model suggests they should. This kind of analysis indicates that the value of $\bar{k}_b$ and its dependence on temperature have meaning only if the pressure is specified and held constant.

C. Reaction Mechanism. The results discussed previously support the energy transfer reaction mechanism of eq 2 for $(CH_3)_3N$ and $(CH_3)_2NH$ and probably for CH_3NH_2. The results are not so clear for NH_3, where detailed agreement between theory and experiment is lacking. There are a number of places where the model used in this paper might break down. It is useful to discuss the possible problems in terms of the assumptions made in the Introduction.

1. All AH^+/A Collisions Result in the Formation of $(A_2H^+)^*$ Complexes. What is meant here by the word "complex" is the most stable configuration of the A_2H^+ system. Also implicit in this assumption, as applied in this paper, is the further assumption that energy is transferred out of the collision coordinate and into the other coordinates of A_2H^+, ultimately obtaining quasi-equilibrium. This assumption could break down in two ways: (a) multiple configurations of A_2H^+ could be formed each with a distinct dissociation energy and lifetime, or (b) quasi-equilibrium does not occur before dissociation. In the systems studied here, problem (a) becomes more likely as the system varies from NH_3 to $(CH_3)_3N$. Since agreement between theory and experiment generally improves in that order, it appears that multiple intermediate structures do not exist in large quantities in these systems. This may not be the case for larger amines, however. Meot-Ner and Field have shown that the apparent value of k_2 for the $C_2H_5(CH_3)_2N$ system levels off at a pressure of about 1 Torr at a value approximately 20% of the collision limit. The implication is that k_f for the formation of complexes that can be stabilized at these pressures is substantially less than the collision limit. At some higher pressure k_2 would have to rise again and eventually level off at $k_{collision}$ because even the shortest lived complexes are stabilized at highest pressures. We have observed similar effects in our laboratories with large ammonium and oxonium ions.[11] Bohme et al.[12] have reported similar effects in the dimerization of N_2^+ with N_2 and O_2^+ using He as the collision gas. In these cases k_2 leveled off at less than 1% of $k_{collision}$. Hence, while it *appears* that multiple complex formation is not a problem in the systems discussed here, caution must be observed in routinely assuming that the assumption is valid.

The problem (b), that quasi-equilibrium does not occur before dissociation of the complex, has been discussed by Neilson et al.[3] Briefly, they noted that the rate of energy transfer out of the collision coordinate competes with the lifetime of the vibration associated with that coordinate. They suggested that k_f had the form

$$k_f = k_{collision}\left(\frac{k_{ET}}{k_{ET} + \tau^{-1}}\right) \quad (26)$$

where k_{ET} is the rate constant for energy transfer out of the reaction coordinate and τ is the lifetime of $(A_2H^+)^*$. Since k_{ET} will increase as the density of states of A_2H^+ increases, and since τ varies only slowly from NH_3 to $(CH_3)_3N$, eq 26 indicates that this effect would be most important for NH_3 and least important for $(CH_3)_3N$. There appears to be no simple way to utilize eq 26 to even qualitatively explain the deviation of experiment and theory in the case of NH_3. In addition to modifying the distribution function $F(E,\mathcal{J})$ for the activating reaction for the formation of complexes (since the fraction in eq 26 is different for each $E,\mathcal{J}$ state), the application of eq 26 also implies that there may be some complexes which will not reach quasi-equilibrium. For these cases $k_b(E,\mathcal{J})$ must be reformulated in terms of dynamical, rather than statistical, arguments. Such a treatment is beyond the scope of the present paper.

Neilson et al.[3] used experimental inverse plots, Figure 6, to obtain "experimental" values of k_f using eq 3b and extrapolation to $p = \infty$. This technique yielded values of k_f substantially lower than $k_{collision}$ that varied from system to system. This method of obtaining k_f ignores the fact that $\bar{k}_b$ is pressure dependent as pointed out by Olmstead et al.[8] and confirmed here. The point is clearly made in Figure 7d. The inverse plot is essentially linear over the portion of the pressure range that corresponds to the ICR experiments of Neilson et al.[3] Extrapolation of the linear portion yields an intercept value of "k_f" = 3×10^{-11} cm^3/s. Neilson et al. reported a value of "k_f" = 3.3×10^{-11} cm^3/s from experimental inverse plots. The value obtained from the actual theoretical intercept in Figure 7d is 1.2×10^{-9} cm^3/s. Hence, the use of inverse plots extrapolated to infinite pressures in the gas phase is a risky business that may give results in error by several orders of magnitude.

2. All $(A_2H^+)^*$/A Collisions Result in Stabilized A_2H^+ Molecules. This is probably a good assumption for the thermal systems discussed in this work. The only exit channel for the complex is back-dissociation to the reactants. Removal of even a significant amount of rotational energy from $(A_2H^+)^*$ should greatly decrease $\bar{k}_b$ and make the lifetime greater than the detection time of the ICR ($1-2 \times 10^{-3}$ s). Recent work in our laboratory[13] on the $(CH_3)_3N$ system indicates that $(CH_3)_3N$ is the best stabilizer for $[(CH_3)_3N]_2H^+$ from among more than 20 atoms and molecules used as collision gases with the single exception of the highly polar molecule HCN which had a stabilization efficiency slightly larger than $(CH_3)_3N$. The variation in relative stabilization from the least efficient (H_2,He) to the most efficient, HCN, was less than a factor of 4, indicating that all systems are reasonably efficient. Hence, this assumption seems well founded.

3. The Ion–Molecule Collision Rate Constants k_f and k_s Are Governed by the Long-Range Potential and Hence Are Given by Langevin[4] or ADO[5] Theory. This assumption is certainly essentially correct. Recent work[14] indicates that the ADO theory may underestimate the collision rate for polar systems by as much as 30% because of simplifying assumptions of this theory, not because the long-range potential does not dominate the collision process. In any case, minor errors in the collision rate constant will have little effect on the results presented here.

In summary, then, there are no readily apparent reasons why theory and experiment deviate in the NH_3 system. Since this system was by far the most difficult to observe experimentally,[3] there may be unusually large or possibly systematic errors in the data. These errors coupled with the rather minor problems with the model noted in this section and previous sections could explain the discrepancies. More experimental data would be required before this point can be finally settled, however.

D. Comparison of Phase Space Theory with RRKM Theory. The essential theoretical difference between the phase space and RRKM formulations of statistical rate theory lies in the method of dealing with angular momentum effects. Phase space theory accounts rigorously for the coupling of all angular momenta at the transition state. This includes, in addition to the orbital motion of the two fragments about their center of mass, the individual rotational motion of the two separate fragments. The RRKM treatment neglects the angular momentum coupling of the individual rotational degrees of freedom with the orbital motion. Thus RRKM theory is identical with phase space theory for the dissociation of a diatomic molecule. For polyatomic species, RRKM theory will be a very good approximation to phase space theory in the limit $\mathcal{J} \to 0$. As angular momentum increases the agreement between RRKM and phase space theories is expected to become worse. The systems studied here were initially considered to be prime candidates for observing the effects of the rigorous treatment of angular momentum mainly because of the large angular momentum distribution expected for the activating reaction. However, the results illustrated in Figure 5 indicate that there is very little difference between the rigorous phase space theory and the approximate RRKM treatment in the pressure–temperature regime examined. Although $F(E,\mathcal{J})$ does extend up to fairly high $\mathcal{J}$ values, the upper end of the $\mathcal{J}$ distribution is essentially lost in the steady-state distribution at the low pressures considered here. Thus, in order to observe the full effect of high angular momentum states it is not only necessary that these states be created by the activation process but also that the experimental pressure is great enough so that these states contribute substantially to the total rate of reaction. Alternatively, a reaction would have to be studied where the full effects of the angular momentum distribution of the activating reaction are felt. Any bimolecular reaction proceeding via a statistical complex would satisfy this requirement. A good example has recently been given by Meisels and co-workers[15] for reaction 27. It was shown that the experimental product

$$C_2H_4^+ + C_2H_4 \rightleftharpoons (C_4H_8^+)^* \begin{cases} \rightarrow C_3H_5^+ + CH_3 & (27a) \\ \rightarrow C_4H_7^+ + H & (27b) \end{cases}$$

distribution of this reaction is substantially different than that of the reaction

$$C_4H_8 + h\nu \longrightarrow (C_4H_8^+)^* + e \begin{cases} \rightarrow C_3H_5^+ + CH & (28a) \\ \rightarrow C_4H^+ + H & (28b) \end{cases}$$

The results were explained by noting the very different angular momentum distributions in the two $C_4H_8^+$ complexes, and good agreement between theory and experiment was obtained on this basis. The theory used by Meisels explicitly included conservation of angular momentum.

V. Summary

The principal points of this paper are these:

(1) Explicit expressions that conserve energy and angular momentum are presented for the distribution function of the activating reaction, $F(E,\mathcal{J})$, and for the steady-state distribution function, $P_{ss}(E,\mathcal{J})$, of $(A_2H^+)^*$.

(2) The microscopic unimolecular rate constant $k(E,\mathcal{J})$ is shown to be a strong function of $\mathcal{J}$.

(3) Reasonably good agreement is obtained between experiment and theory for A = CH_3NH_2, $(CH_3)_2NH$, and

Table II. Estimated Structures for Calculation of Rotational Constants[c]

	NH_3		NH_4^+		NH_3-H^+-NH_3	
N-H	1.008[a]		1.034[a]		1.034	
N-H^+					1.060	
	∡HNH	107.3[a]		109.5		109.5
	CH_3NH_2		$CH_3NH_3^+$		CH_3NH_2-H^+-CH_3NH_2	
H-N	1.014[a]		1.040		1.040	
C-N	1.474[a]		1.474		1.474	
C-H	1.093		1.093		1.093	
N-H^+					1.066	
	∡HNH	105.8[a]		106.2		106.2
	∡CNH	112.1[b]		112.5		112.5
	∡HCH	109.5[a]		109.5		109.5
	∡HCN	109.5		109.5		109.5
	$(CH_3)_2NH$		$(CH_3)_2NH_2^+$		$(CH_3)_2NH$-H^+-$(CH_3)_2NH$	
N-H	1.020		1.046		1.046	
C-N	1.472		1.472		1.472	
C-H	1.077		1.077		1.077	
N-H^+					1.073	
	∡HNH			103.0		103.0
	∡CNH	109.0		109.5		109.5
	∡HCH	109.5		109.5		109.5
	∡HCN	109.5		109.5		109.5
	∡CNC	113.0		115.1		115.1
	$(CH_3)_3N$		$(CH_3)_3NH^+$		$(CH_3)_3N$-H^+-$(CH_3)_3N$	
N-H			1.052		1.052	
C-N	1.47[a]		1.47		1.47	
C-H	1.06[a]		1.06		1.06	
N-H^+					1.078	
	∡CNH			108.4		108.4
	∡HCH	109.5[a]		109.5		109.5
	∡HCN	109.5		109.5		109.5
	∠CNC	108.0[a]		110.5		110.5

[a] Reference 25. [b] Reference 16. [c] Unreferenced values estimated as described in text. Bond lengths in ångstroms; bond angles in degrees.

$(CH_3)_3N$. For A = NH_3, the agreement is not as good. Either the model seriously breaks down in this case or the experimental data are inaccurate.

(4) A thorough discussion of the energy-transfer model is given, with a focus on how to best compare experiment to theory. The use of "inverse" plots of the type k_2^{-1} vs. A^{-1} to obtain either $\bar{k}_b$ from the slope or k_f from the intercept at $A = \infty$ can yield misleading results. This is especially true for k_f, where it is shown that this method can be in error by several orders of magnitude.

Acknowledgment. The authors gratefully acknowledge the support of the National Science Foundation under Grant CHE77-15449 and the donors of the Petroleum Research Fund, administered by the American Chemical Society, for partial support of this research.

Appendix. Parameters Used in Rate Calculations for the Proton-Bound Amine Dimers

Literature values are available for all the vibrational modes in ammonia,[16] ammonium ion,[16] methylamine,[17] and all modes except the torsional oscillation in methylammonium ion (from the IR spectra of methylammonium chloride).[18] There is also data available on the torsional and skeletal modes of the larger species obtained from the Raman spectra of aqueous amines and ammonium chlorides[19] and from the gas-phase IR spectra of the neutrals.[20] The remaining oscillator frequencies in the amines and ammonium ions were estimated from the trends in the known data and from values for the corresponding alkanes. For the proton-bound dimers all nonskeletal modes were assumed equal to the corresponding modes in the protonated amines. The two N-H^+-N stretching modes have been calculated for the ammonia dimer in an ab initio study of the $N_2H_7^+$ potential energy surface.[21] The corresponding stretching frequencies for the other dimers can be calculated using standard relationships for XY_2 molecules.[22] Each dimer has one free internal rotation whose moment of inertia was calculated from an assumed structure (see below). The remaining skeletal frequencies were chosen so that the entropy, ΔS, for the reaction A + $AH^+ \rightleftarrows A_2H^+$ calculated from statistical mechanics[23] matched that determined experimentally.[24] This procedure has been discussed by Forst.[16]

Literature values[16] for rotational constants were used where available, but in most cases these parameters were calculated

Table III. Parameters Used for the Ammonia System

	NH_3		NH_4^+		NH_3-H^+-NH_3	
ν_i[a]	3400 (3)	[19]	3100 (4)	[19]	3000 (6)	
	1628 (2)	[19]	1685 (2)	[19]	1676	[24]
	950	[19]	1397 (3)	[19]	1578 (4)	
					1434 (2)	
					954 (4)	
					668	[24]
					105 (2)	
B_i[b]					11.731	
σ_i[c]					3	
B[b]	8.539		5.865		0.7302	
σ[c]	3		12		6	
α[d]	2.34					
ΔS_{550}[e]	−25.8					
E_0[f]	24.0					

[a] Vibrational frequencies in cm^{-1}; degeneracies in parentheses; brackets indicate appropriate reference; higher frequencies have been rounded; unreferenced values estimated as in text. [b] Rotational constant in cm^{-1}; calculated from structure in Table II; i indicates internal rotation. [c] Symmetry number for rotation; i indicates internal rotation. [d] Polarizability in $Å^3$. [e] Experimental entropy change in cal/deg for the reaction $AH^+ + A \rightleftarrows A_2H^+$ (ref 24). [f] Well depth in kcal/mol calculated as explained in text.

Table IV. Parameters Used for the Methylamine System

	CH_3NH_2		$CH_3NH_3^+$		$(CH_3NH_2)_2H^+$
ν_i[a]	3400 (2)	[20]	3000 (3)	[21]	3000 (4)
	2920 (3)	[20]	2950 (3)	[21]	2950 (6)
	1623	[20]	1578 (2)	[21]	1665
	1465 (3)	[20]	1450 (3)	[21]	1462 (2)
	1419	[20]	1434	[21]	1450 (6)
	1165 (2)	[20]	1265 (2)	[21]	1338 (2)
	1044	[20]	1004	[21]	1278 (2)
	780	[20]	954 (2)	[21]	1265 (4)
	268	[20]	289		1004 (2)
					748 (2)
					495
					289 (2)
					105 (2)
					95 (2)
B_i[b]					1.146
σ_i[c]					1
B[b]	1.241		1.096		0.1771
σ[c]	1		3		2
α[d]	4.18				
ΔS_{550}[e]	−23.6				
E_0[f]	22.4				

[a]–[f] See Table III for notes.

Table V. Parameters Used for the Dimethylamine System

	$(CH_3)_2NH$		$(CH_3)_2NH_2^+$		$((CH_3)_2NH)_2H^+$
ν_i[a]	3400		3000 (2)		3000 (2)
	2920 (6)		2950 (6)		2950 (12)
	1465 (6)		1462		1661
	1165 (4)		1450 (6)		1450 (12)
	1078	[22]	1338		1265 (8)
	931	[22]	1278		1029 (2)
	730 (2)	[23]	1265 (4)		895 (2)
	383	[23]	1029	[22]	650 (4)
	256	[23]	895	[22]	411 (3)
	230	[23]	748		268 (2)
			412	[22]	260 (4)
			268		216 (2)
			216		105 (2)
B_i[b]					0.4903
σ_i[c]					1
B[b]	0.4599		0.4320		0.0827
σ[c]	1		2		2
α[d]	5.92				
ΔS_{550}[e]	−25.7				
E_0[f]	23.2				

[a-f] See Table III for notes.

Table VI. Parameters Used for the Trimethylamine System

	$(CH_3)_3N$		$(CH_3)_3NH^+$		$((CH_3)_3N)_2H^+$
ν_i[a]	2920 (9)		3000		2950 (18)
	1465 (9)		2950 (9)		1659
	1165 (6)		1450 (9)		1450 (18)
	1036 (2)	[22]	1265 (6)		1265 (12)
	827	[22]	987 (2)	[22]	987 (4)
	426 (2)	[23]	821	[22]	821 (2)
	366	[23]	650 (2)		407 (6)
	262 (3)	[23]	407 (3)	[22]	359
			260 (3)		260 (6)
					225 (4)
					105 (2)
B_i[b]					0.3298
σ_i[c]					3
B[b]	0.2458		0.2357		0.0562
σ[c]	3		3		6
α[d]	7.92				
ΔS_{550}[e]	−32.0				
E_0[f]	23.6				

[a-f] See Table III for notes.

from assumed structures. Note that all species are treated as spherical tops, using the geometric mean of the three-component rotational constants. It has been shown that the errors introduced in phase space calculations by use of these approximations are usually small.[10]

Structural parameters (bond lengths and bond angles) were obtained from the usual sources[16,25] for NH_3, CH_3NH_2, $(CH_3)_3N$, and NH_4^+. Values for the remaining species were estimated from the trends in the above compounds. The dimers were assumed to have the same structures as the protonated amines, except for the N-H^+ bond lengths, which were assumed to increase from protonated amine to dimer by the same amount that the corresponding N-H bond increased from amine to protonated amine.

The difference in zero-point energies at 0 K, E_0, was chosen so that the calculated statistical-mechanical[23] ΔH for the reaction agreed with the experimental value[24] at the experimental temperature.

A summary of all the data used in the calculations is shown in Tables II-VI.

References and Notes

(1) (a) P. J. Robinson and K. A. Holbrook, "Unimolecular Reactions", Wiley-Interscience, New York, 1972; (b) W. Forst, "Theory of Unimolecular Reactions", Academic Press, New York, 1973.
(2) M. Meot-Ner and F. H. Field, *J. Am. Chem. Soc.*, **97**, 5339 (1975).
(3) P. V. Neilson, M. T. Bowers, M. Chau, W. R. Davidson, and D. H. Aue, *J. Am. Chem. Soc.*, **100**, 3649 (1978).
(4) P. Langevin, *Ann. Chim. Phys.*, **5**, 245 (1905); G. Gioumousis and D. P. Stevenson, *J. Chem. Phys.*, **29**, 294 (1958); E. Vogt and G. H. Wannier, *Phys. Rev.*, **95**, 1190 (1954).
(5) T. Su and M. T. Bowers, *J. Chem. Phys.*, **58**, 3027 (1973); *Int. J. Mass Spectrom. Ion Phys.*, **17**, 309 (1975); L. Bass, T. Su, W. J. Chesnavich, and M. T. Bowers, *Chem. Phys. Lett.*, **34**, 119 (1975).
(6) R. A. Marcus and O. K. Rice, *J. Phys. Colloid Chem.*, **55**, 894 (1951); G. M. Wieder and R. A. Marcus, *J. Chem. Phys.*, **37**, 1835 (1962); R. A. Marcus, *ibid.*, **20**, 359 (1952).
(7) H. B. Rosenstock, M. B. Wallenstein, A. L. Wahrhaftig, and H. Eyring, *Proc. Natl. Acad. Sci. U.S.A.*, **38**, 667 (1952).
(8) W. N. Olmstead, M. Lev-On, D. M. Golden, and J. I. Brauman, *J. Am. Chem. Soc.*, **99**, 992 (1977).
(9) (a) P. Pechukas and J. C. Light, *J. Chem. Phys.*, **42**, 3281 (1965); J. Lin and J. C. Light, *ibid.*, **43**, 3209 (1965); J. C. Light, *Discuss. Faraday Soc.*, **44**, 14 (1967); (b) E. Nikitin, *Teor. Eksp. Khim.*, **1**, 135, 144, 428 (1965); *Theor. Exp. Chem.*, **1**, 83, 90, 275 (1965).
(10) W. J. Chesnavich and M. T. Bowers, *J. Chem. Phys.*, **66**, 2306 (1977); *J. Am. Chem. Soc.*, **98**, 8301 (1976); W. J. Chesnavich, Ph.D. Thesis, University of California, Santa Barbara, 1976.
(11) W. R. Davidson, P. V. Neilson, M. T. Bowers, and D. H. Aue, unpublished results.
(12) D. K. Bohme, D. B. Dunkin, F. C. Fehsenfeld, and E. E. Ferguson, *J. Chem. Phys.*, **49**, 5201 (1968); **51**, 863 (1969).
(13) R. D. Cates and M. T. Bowers, unpublished work.
(14) W. J. Chesnavich, T. Su, and M. T. Bowers, in "Kinetics of Ion-Molecule Reactions", P. Ausloss, Ed., Plenum Press, New York, 1979; *J. Chem. Phys.*, in press.
(15) G. G. Meisels, private communication.
(16) G. Herzberg, "Molecular Spectra and Molecular Structure", Vol. II, Van Nostrand, Princeton, N.J., 1945.
(17) T. Shimanouchi, "Tables of Molecular Vibrational Frequencies", Consolidated Vol. I, National Bureau of Standards, Washington, D.C., 1972.
(18) A. Cabana and C. Sandorfy, *Spectrochim. Acta*, **18**, 843 (1962).
(19) J. T. Edsall, *J. Chem. Phys.*, **5**, 225 (1937).
(20) W. G. Fately and F. A. Miller, *Spectrochim. Acta*, **18**, 977 (1962).
(21) P. Merlet, S. D. Peyerimhoff, and R. J. Buenker, *J. Am. Chem. Soc.*, **94**, 8301 (1972).
(22) Reference 19, pp 172, 187.
(23) See, for example, B. J. McClelland, "Statistical Thermodynamics", Chapman and Hall, London, 1973.
(24) J. D. Payzant, A. J. Cunningham, and P. Kebarle, *Can. J. Chem.*, **51**, 3242 (1973).
(25) "Handbook of Chemistry and Physics", 56th ed., R. C. Weast, Ed., Chemical Rubber Publishing Co., Cleveland, Ohio, 1975.